

Dependence of Hole Concentration in p-Type Silicon Solar Cell Wafers on Temperature and on Position within the Polycrystalline Ingot

H. Matsuura, T. Ishida, K. Nishikawa, N. Fukunaga and T. Kuroda

Department of Electronic Engineering and Computer Science
Osaka Electro-Communication University
18-8 Hatsu-cho, Neyagawa, Osaka 572-8530, Japan

Keywords: Impurity, Polycrystalline Silicon Ingot, Solar Cell, Temperature Dependent Hole Concentration

Abstract. Conversion efficiency of polycrystalline silicon pn solar cells, which are fabricated using wafers sliced out of B-doped p-type poly-Si ingots, strongly depends on where it is taken from within the ingot. Since the wafers near the bottom or top of the ingot cannot be used for commercial solar cells, the relationship between the conversion efficiency and the temperature dependence of the hole concentration in poly-Si wafers is investigated. It is found that the hole concentrations are classified into three categories. In wafers near the bottom of the ingot it is abnormal because it shows a peak, while the behavior in wafers near the top results from the incorporation of another acceptor species into the wafers or the creation of defects in the wafers besides B acceptors.

Introduction

In order to avoid global warming, solar cells are appropriate for the generation of electricity. Although single crystalline silicon (c-Si) and III-V compound semiconductors have been studied as materials for high conversion efficiency (η) solar cells, polycrystalline silicon (poly-Si) solar cells are suitable for terrestrial solar cells because of reasonable price and moderate η . Although commercial poly-Si pn solar cells are usually fabricated from p-type wafers sliced out of B-doped poly-Si ingots, the η of poly-Si pn solar cells strongly depends on where it is taken from within the ingot. This indicates that the wafers near the bottom or top of the ingot cannot be used for commercial solar cells. In order to lower the price of poly-Si solar cells, therefore, almost all wafers sliced out of the ingot should be used.

In order to investigate the relationship between η and the electric properties of B-doped p-type poly-Si wafers, the temperature dependence of the hole concentration $p(T)$ in the wafer is measured, and the dependence of $p(T)$ on the position of the wafer within the ingot is studied. The densities and energy levels of acceptors or defects in the wafers are determined using free carrier concentration spectroscopy (FCCS) [1,2,3], which can graphically determine the densities and energy levels of impurities and defects in a semiconductor from $p(T)$.

Free Carrier Concentration Spectroscopy

FCCS is a graphical peak analysis method for determining the densities and energy levels of several dopant species without any assumption regarding dopant species, while the number of dopant species should be assumed beforehand in the case of a least-squares fit of the charge neutrality equation to $p(T)$ [4,5]. Using an experimental $p(T)$, the FCCS signal is defined as [1,2,3]

$$H(T, E_{\text{ref}}) \equiv \frac{p(T)^2}{(kT)^{5/2}} \exp\left(\frac{E_{\text{ref}}}{kT}\right). \quad (1)$$

The FCCS signal has a peak at the temperature corresponding to each acceptor level, where E_{ref} is the

parameter that can shift the peak temperature of $H(T, E_{\text{ref}})$ within the temperature range of the measurement, k is the Boltzmann constant and T is the absolute temperature. From each peak, the density and energy level of the corresponding acceptor species can be accurately determined [6]. On the other hand, the FCCS signal is theoretically derived as [1,2,3]

$$H(T, E_{\text{ref}}) = \sum_{i=1} \frac{N_{Ai}}{kT} \exp\left(-\frac{\Delta E_{Ai} - E_{\text{ref}}}{kT}\right) I(\Delta E_{Ai}) + \frac{\Delta N_A N_{V0}}{kT} \exp\left(\frac{E_{\text{ref}} - \Delta E_F}{kT}\right), \quad (2)$$

where

$$I(\Delta E_{Ai}) = \frac{N_{V0}}{4 + \exp\left(-\frac{\Delta E_{Ai} - \Delta E_F}{kT}\right)}, \quad (3)$$

$$N_V(T) = N_{V0} k^{3/2} T^{3/2}, \quad (4)$$

$$N_{V0} = 2 \left(\frac{2\pi m_h^*}{h^2} \right)^{3/2}, \quad (5)$$

$$\Delta N_A = N_{A0} - N_D, \quad (6)$$

$$\Delta E_F = kT \ln \left[\frac{N_V(T)}{p(T)} \right], \quad (7)$$

N_{Ai} and ΔE_{Ai} are the i -th acceptor density and the i -th acceptor level measured from E_V , respectively, ΔE_F is the Fermi level measured from E_V , N_{A0} is the density of acceptors completely ionized below the temperature range of the measurement, N_D is the donor density, $N_V(T)$ is the effective density of states in the valence band, h is Planck's constant, and m_h^* is the hole effective mass.

Experimental

After scrap c-Si with a trace of B was melt at 1500 °C in a silica crucible in an Ar atmosphere, a p-type poly-Si ingot with 69 cm in length, 69 cm in width and 21 cm in height was recrystallized at 1400 °C. The ingot was horizontally sliced into 300- μm -thick poly-Si wafers, and then the surfaces of the wafers were polished.

The sample was cut into a square $1 \times 1 \text{ cm}^2$ in size from the central part of the wafer in order to avoid the influence of four sides of the ingot. The number of grains in each sample was 5 to 7, and the grain size in each wafer was similar. Ohmic metal (Au with 1 % Ga) was deposited on four corners of the surface, and then the sample was annealed at 400 °C in an Ar atmosphere for 1 min in order to obtain good Ohmic contacts. The $p(T)$ was measured by the van der Pauw method at temperatures between 80 and 420 K and in a magnetic field of 1.4 T.

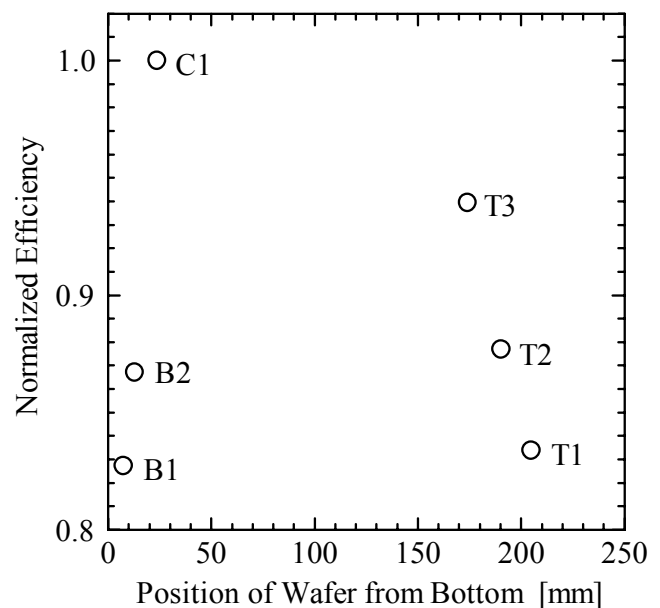


Fig. 1 Dependence of normalized conversion efficiency on position of wafer from bottom.

Results and Discussion

Figure 1 shows the dependence of η of the poly-Si pn solar cell on the position of the wafer within the ingot, where each η was normalized using the highest η in C1. In the figure, the relationship between the sample number and the wafer position is indicated. The wafers located between C1 and T3 can be used for commercial solar cells. On the other hand, the η decreases rapidly with approaching the bottom or top of the ingot.

Figure 2 displays the hole concentration $p(300)$ and the hole mobility $\mu_p(300)$ at room temperature. The $p(300)$ increases and the $\mu_p(300)$ decreases with approaching the bottom of the ingot, while both the $p(300)$ and the $\mu_p(300)$ increase with approaching the top. This suggests that the origin that lowers η in the wafers near the bottom is different from that in the wafers near the top.

Figure 3 shows a set of six $p(T)$ in wafers at different positions of the ingot, where the $p(T)$ in C1 corresponds to the highest η solar cell (open circles). The $p(T)$ in the wafers near the top (T1: solid squares, T2: open inverted triangles, T3: solid diamonds) increase monotonously with an increase of temperature, indicating that the behavior is normal. However, the $p(T)$ in the wafers near the bottom (B1: open squares, B2: solid triangles) shows a peak, suggesting that the behavior is quite abnormal. As far as we know, this behavior has not been reported yet. The grain sizes in the wafers near the bottom are similar to those in the wafers near the top.

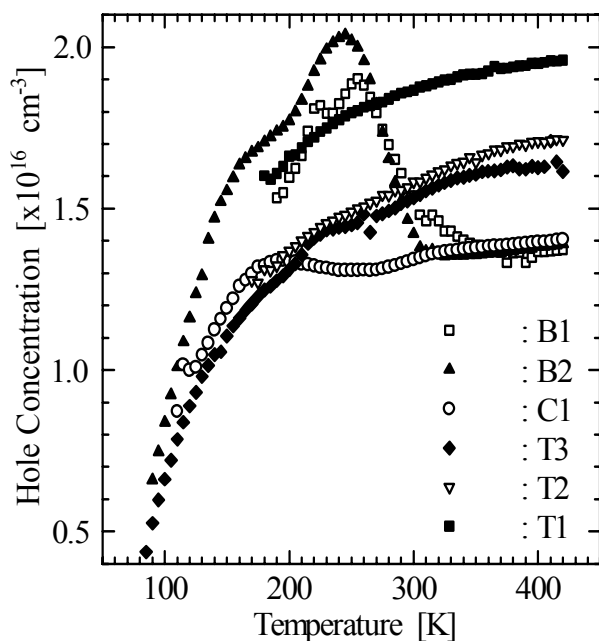


Fig. 3 A set of six $p(T)$ in wafers at different positions.

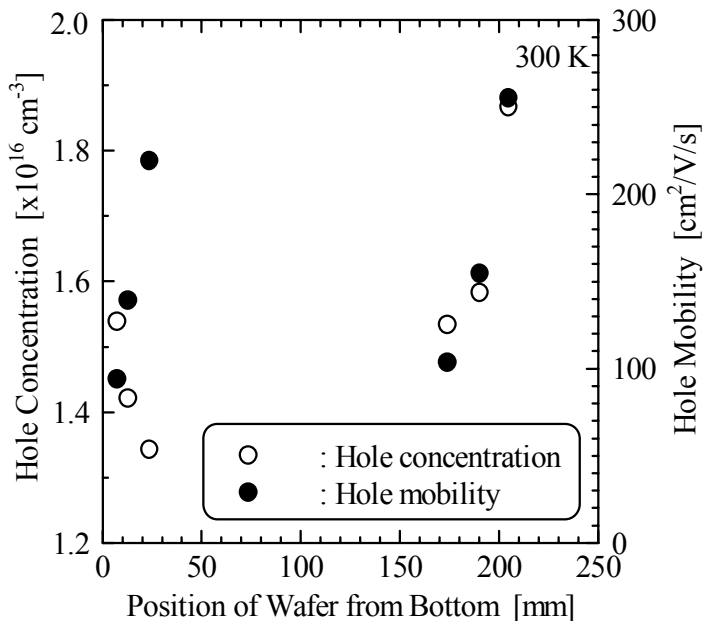


Fig. 2 Dependence of hole concentration and hole mobility at 300 K on position of wafer.

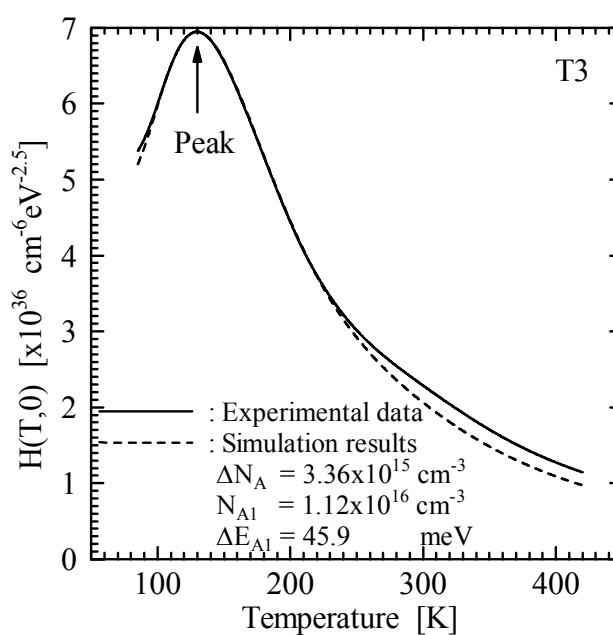


Fig. 4 Experimental and simulated $H(T,0)$ in T3.

Since the $p(T)$ in T1, T2 and T3 are normal, the densities and energy levels of acceptors can be determined. In the FCCS analyses, $H(T, E_{\text{ref}})$ is calculated by interpolating $p(T)$ with a cubic smoothing natural spline function at intervals of 0.1 K. In Fig. 4, the solid curve represents the experimental $H(T, E_{\text{ref}})$ with $E_{\text{ref}} = 0$ eV in T3. The peak temperature and peak value of $H(T, 0)$ are 129.7 K and $6.95 \times 10^{36} \text{ cm}^{-6} \text{ eV}^{-2.5}$, respectively. At temperatures near this peak, the FCCS signal in Eq. (2) can be approximately rewritten as

$$H(T, E_{\text{ref}}) \cong \frac{N_{\text{A1}}}{kT} \exp\left(-\frac{\Delta E_{\text{A1}} - E_{\text{ref}}}{kT}\right) I(\Delta E_{\text{A1}}) + \frac{\Delta N_{\text{A}} N_{\text{V0}}}{kT} \exp\left(\frac{E_{\text{ref}} - \Delta E_{\text{F}}}{kT}\right), \quad (8)$$

because deep acceptors can hardly emit holes to the valence band. From this peak, the values of N_{A1} and ΔE_{A1} are determined to be $1.12 \times 10^{16} \text{ cm}^{-3}$ and 45.9 meV, respectively, and also ΔN_{A} is evaluated to be $3.36 \times 10^{15} \text{ cm}^{-3}$. In Fig.4, the broken curve represents the $H(T, 0)$ simulated using the obtained ΔN_{A} , N_{A1} and ΔE_{A1} , which is in good agreement with the solid curve at temperatures near the peak. At >200 K, however, the solid curve is greater than the broken curve, indicating that there exist deep acceptor species in T3.

In order to evaluate the deep acceptors, a function that is not influenced by ΔN_{A} , N_{A1} and ΔE_{A1} can be introduced as

$$H2(T, E_{\text{ref}}) \cong \frac{p(T)^2}{(kT)^{5/2}} \exp\left(\frac{E_{\text{ref}}}{kT}\right) - \frac{N_{\text{A1}}}{kT} \exp\left(-\frac{\Delta E_{\text{A1}} - E_{\text{ref}}}{kT}\right) I(\Delta E_{\text{A1}}) - \frac{\Delta N_{\text{A}} N_{\text{V0}}}{kT} \exp\left(\frac{E_{\text{ref}} - \Delta E_{\text{F}}}{kT}\right), \quad (9)$$

which is derived from Eqs. (1) and (2). Figure 5 shows the experimental $H2(T, E_{\text{ref}})$ calculated by Eq. (9) using the obtained ΔN_{A} , N_{A1} and ΔE_{A1} . The peak temperature and peak value of $H2(T, 0)$ are 321.1 K and $2.36 \times 10^{35} \text{ cm}^{-6} \text{ eV}^{-2.5}$, respectively, from which N_{A3} and ΔE_{A3} are determined to be $2.99 \times 10^{15} \text{ cm}^{-3}$ and 129.0 meV, respectively. Here, the acceptor is called a 3rd acceptor because it will be found that there exists a ~ 80 meV acceptor in T1 and T2.

In order to verify the obtained ΔN_{A} , N_{A1} , ΔE_{A1} , N_{A3} and ΔE_{A3} , the $p(T)$ is simulated using the obtained values. In Fig. 6, the open circles and solid curve represent the experimental and simulated $p(T)$, respectively. The simulated $p(T)$ is quantitatively in good agreement with the experimental $p(T)$, indicating that the values obtained by FCCS are reliable.

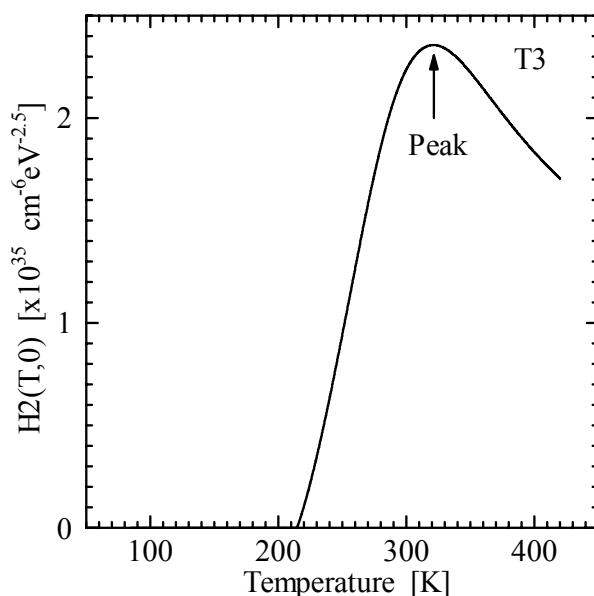


Fig. 5 Experimental $H2(T, 0)$ obtained using Eq. (9).

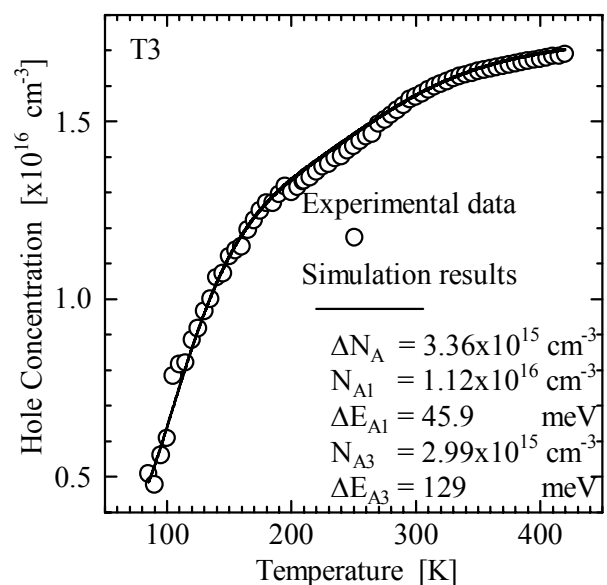


Fig. 6 Comparison of simulated $p(T)$ with experimental $p(T)$ in T3.

Table I: Results obtained by FCCS.

		a) These values are determined using $p(T)$ at <170 K.			b) These values are $\Delta N_A + N_{A1}$.	
Sample Number		B2	C1	T3	T2	T1
1 st acceptor	ΔN_A [$\times 10^{16} \text{ cm}^{-3}$]			0.336		
	N_{A1} [$\times 10^{16} \text{ cm}^{-3}$]	2.16 ^(a)	1.51 ^(a)	1.12	1.09 ^(b)	1.45 ^(b)
	ΔE_{A1} [meV]	40.3 ^(a)	38.4 ^(a)	45.9		
2 nd acceptor	N_{A2} [$\times 10^{16} \text{ cm}^{-3}$]				0.602	0.490
	ΔE_{A2} [meV]				80.7	82.8
3 rd acceptor	N_{A3} [$\times 10^{16} \text{ cm}^{-3}$]			0.299		
	ΔE_{A3} [meV]			129.0		
4 th acceptor	N_{A4} [$\times 10^{16} \text{ cm}^{-3}$]				0.0981	0.0720
	ΔE_{A4} [meV]				188.1	188.8

Since ΔE_{A1} of 45.9 meV is close to the acceptor level (45 meV) of B in Si [7], the 1st acceptor arises from the doped B acceptor. Besides the doped B acceptor, there is very shallow acceptor as well as another deep acceptor at 129 meV.

In the same way as illustrated for T3, the densities and energy levels of acceptors in T1 and T2 are determined. The obtained results are listed in Table I. Since the $p(T)$ in T1 and T2 could not be measured under ~ 180 K, it is impossible to determine ΔN_A , N_{A1} and ΔE_{A1} . However, the total density of acceptors at < 80 meV can be determined. Different from the case of T3, there are two deep acceptor species such as ~ 80 meV and ~ 188 meV acceptors. The ~ 90 meV, ~ 130 meV and ~ 190 meV defects were reported by Matsuura et al. [8], and the origins of the defects at ~ 90 meV and ~ 190 meV are considered to be a carbon-related complex (C_i-C_s) and a divacancy (V-V), respectively. The energy level of an iron-boron complex (Fe-B) is reported to be ~ 100 meV [9]. At the present time, it is difficult to determine these origins.

As is clear from Fig. 3, the behavior of $p(T)$ in B1 or B2 is abnormal because the $p(T)$ shows a peak. Moreover, the values of the $p(T)$ above 300 K are close to those in C1. Using the $p(T)$ at < 170 K, the acceptor density and acceptor level are determined by FCCS, which are listed in Table I.

As is clear from Table I, the B acceptor density in B2 is higher than that in C1, while the density of all the acceptor species in the wafers near the top is higher than that in C1 and it increases with approaching the top.

Figure 7 displays the temperature dependence of the hole mobility $\mu_p(T)$ in B1 (open squares), B2 (solid triangles) and C1 (open circles). The $\mu_p(T)$ in B1 or B2 decreases and then increases with increasing temperature, and finally decreases again with temperature. This behavior is also abnormal. On the other hand, the $\mu_p(T)$ in C1 corresponding to high η decreases monotonously with an increase of temperature.

In order to determine whether the abnormal

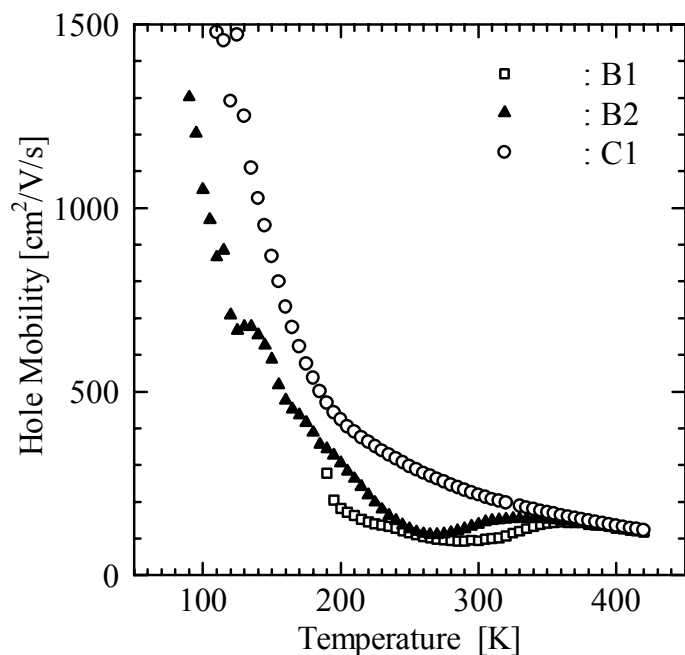


Fig. 7 A set of three $\mu_p(T)$ for wafers near bottom of ingot.

behavior of $p(T)$ or $\mu_p(T)$ was thermally stable, Hall-effect measurements were carried out from high temperature to low temperature (backward measurement) after they were done from low temperature to high temperature (forward measurement). Figure 8 shows $p(T)$ and $\mu_p(T)$ in B2 corresponding to the forward and backward measurements. Since both the results are similar to each other, the behavior is thermally stable. The investigation of origin causing the behavior is now in progress

Conclusion

The temperature dependence of the hole concentration in wafers sliced out of B-doped poly-Si ingots was investigated, because the conversion efficiency of poly-Si pn solar cells strongly depended on where it was taken from within the ingot. Although the wafers near the bottom or top of the ingot could not be used for commercial solar cells because of low conversion efficiency, the origins lowering the efficiency were quite different. The $p(T)$ in wafers near the top of the ingot showed normal behavior, while the $p(T)$ in wafers near the bottom showed abnormal behavior because it showed a peak. The acceptor density increased with approaching the top or bottom. However, the increase in the acceptor density resulted from the incorporation of deep acceptors or defects to the wafers near the top, while it arose from the increase in B acceptors in the wafers near the bottom.

References

- [1] H. Matsuura, Y. Masuda, Y. Chen and S. Nishino, Jpn. J. Appl. Phys. **39**, 5069 (2000).
- [2] H. Matsuura, Y. Uchida, N. Nagai, T. Hisamatsu, T. Aburaya and S. Matsuda, Appl. Phys. Lett. **76**, 2092 (2000).
- [3] H. Matsuura, K. Morita, K. Nishikawa, T. Mizukoshi, M. Segawa and W. Susaki, Jpn. J. Appl. Phys. **41**, 495 (2002).
- [4] A. Suzuki, A. Uemoto, M. Shigeta, K. Furukawa and S. Nakajima, Appl. Phys. Lett. **49**, 450 (1986).
- [5] P. S. Dutta, V. Prasad, H. L. Bhat and V. Kumar, J. Appl. Phys. **80**, 2847 (1996).
- [6] The Windows application software for FCCS can be freely downloaded at our web site. (<http://www.osakac.ac.jp/labs/matsuura/>).
- [7] S. M. Sze, *Physics of Semiconductor Devices*, 2nd ed. (Wiley, New York, 1981) p. 21.
- [8] H. Matsuura, Y. Uchida, T. Hisamatsu and S. Matsuda, Jpn. J. Appl. Phys. **37**, 6034 (1998).
- [9] G. Zoth and W. Bergholz, J. Appl. Phys. **67**, 6764 (1990).

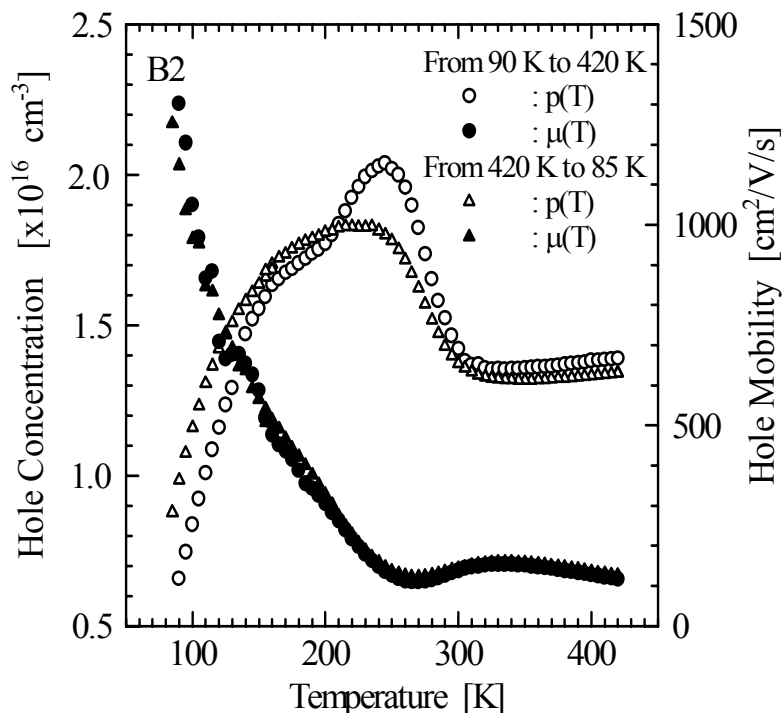


Fig. 8 $p(T)$ and $\mu_p(T)$ measured from low to high temperatures or from high to low temperatures.